Journal of Marine Science and Application (2026) 25: 587-599
https://doi.org/10.1007/s11804-025-00625-4

RESEARCH ARTICLE

Numerical Investigations on Oblique Water Entry Dynamics of an Autonomous Underwater Vehicle Impacting Water Surface

B. Sairam Prasad[1] and G. Ravi Kiran Sastry[1]

Received: 27 December 2024 / Accepted: 04 March 2025

Abstract
This study conducts a detailed numerical investigation into the oblique water entry dynamics of an autonomous underwater vehicle (AUV) impacting the water surface based on the fundamentals of water entry dynamics. It integrates recent advancements in numerical simulations to address the challenges of transient motion and fluid-structure interactions. This study uses advanced computational fluid dynamics (CFD) simulations to explore the complex interaction between the vehicle and the surrounding fluid during the critical transition from air to water. The primary objectives of this investigation include the assessment of resultant forces and the identification of optimal launch parameters such as entry velocity and entry angle to enhance entry effectively. The numerical methodology and results offer valuable insight into the hydrodynamic behavior of AUVs, thereby contributing to more advanced and capable air-launched AUV systems.

Keywords Autonomous underwater vehicles; Hydrodynamics; Computational fluid dynamics; Hydrodynamic forces; Vehicle stability

1 Introduction

Autonomous underwater vehicles (AUVs) are self-propelled vehicles designed to operate in underwater environments for a wide range of applications. These are equipped with advanced sensors and navigating systems enabling them to operate without human intervention. One of the critical challenges in AUV operations is their interaction with the underwater environment, particularly during deployment and recovery. The dynamics of an AUV impacting the water surface are complex and involve significant hydrodynamic forces. Understanding the behavior during water entry is essential in enhancing maneuverability, stability, and performance. This study investigates the water impact of a freely falling AUV using numerical analysis, contributing to the optimization of AUV design for improved underwater performance (Sahoo et al., 2019; Prasad et al., 2024).

The initial theoretical study on water entry impact conducted by Karman (1929) was focused on landing a seaplane on water, based on the law of conservation of momentum and added mass system, which further helps in understanding the phenomenon of water entry. May (1952) conducted numerous experiments, considering the effects of pressure, density, Froude's number, Weber number, Bond number, impact velocity, and water entry angle. Gaudet (1998) studied the effects of low Froude's number and cavity evolution mechanism of circular disks entering the water and observed good agreements in numerical and experimental approaches. Wang et al. (2021) reported that to reduce the time and distance of AUV to be in a horizontal position by varying water entry velocities, water entry angles, nose shapes, and rudder deflection angles and reported that a decrease in time and distance could be done when the rudder angle deflects in a counter-clockwise direction, with an increase in water entry velocity, with smaller nose radius. Shi et al. (2000) used rifles to record a sequence of vertical water entry experiments emphasizing the unsteady flow phenomena such as water splash back, backflow, and cavitation flow and established a relation between the trajectory deviation and water depth. In further studies, Truscott et al. (2014) performed water entry of bullets with various shapes to analyze the deflection of the water entry tra-

Article Highlights

- This study investigates the water impact dynamics of air-launched Autonomous underwater vehicles (AUVs), focusing on fluid structure interactions during air-to-water transition.
- The research evaluates the hydrodynamic behavior of AUVs for different entry angles and velocities to enhance maneuverability.
- This article offers valuable insights into the hydrodynamic behavior of AUVs, contributing to the development of more effective deployment strategies and advancements in underwater technology.

✉ G. Ravi Kiran Sastry
grksastry@nitandhra.ac.in

[1] Department of Mechanical Engineering, NIT Andhra Pradesh, Tadepalligudem, AP 534101, India

jectory and established that a model with a large slenderness ratio and a blunt head is capable of stable underwater movement. Chen et al. (2019) focused on the cavitation visualization of off-axis tip penetrators deployed under high-speed imaging during the water entry phase to capture the water entry angle and the loss of cavitation for different head shapes. The results showed that the change in the water entry head shape played a major role in the deviation of the water entry trajectory. It further supported the work of Chen et al. (2017) who reported the effects of various rudder angles on the trajectory and reported that an increase in rudder angle enhances the vehicle's deflection capabilities. Wang et al. (2022) combined physical and computational mechanics to study the water impact of the air-launched AUVs and their findings asserted that the magnitude of the mechanically induced water impact of the AUV was second-order to the water entry velocity and was directly proportional to the water entry angle.

Choe and Kim (2022) evaluated the pitching characteristics of supercavitating vehicles. They developed a supercavity maneuvering model that incorporates gravity, angle of attack, and inertial forces, and also developed a numerical algorithm to simulate the pitching motions of a maneuverable vehicle during high-speed motion based on the model. Yuan and Xing (2016) conducted natural cavitating flow simulations to analyze how changes in the angle of attack and cavitation number affect the flow pattern together with hydrodynamic forces in control fin-fitted vehicles. Guo and Zou (2017) performed computational fluid dynamics (CFD) simulations of the ventilated supercavity surrounding a cylindrical body with cavitation. Within the framework of the computational results, they focused on the internal cavity velocities to study the gas loss mechanisms of the ventilated supercavity. Fronzeo et al. (2019) studied ventilated cavities as a disk cavitator producing ventilated cavities and studied the variations of pressure inside the ventilated cavities. Zheng et al. (2020) performed computations of buoyant rotors with ventilated cavitating flows around a constructed body. From the computed results, the transient features of vortex-cavitation interaction were examined in a detailed way. Zhang et al. (2022) carried out experimental and computational studies on the unsteady behavior of ventilated cavitating flows over an axisymmetric body and explored the flow physics around the ventilated cavity with and without the angle of attack. Tan et al. (2019) carried out the unsteady flow behavior and force distribution of an underwater vehicle during various stages of the exit process. Amiri et al. (2019) investigated the impact of free-surface effects on an AUV for the mentioned angle of drift and found that for specific submersion ratios, the effect is negligible. Yan et al. (2018) investigated the water entry of air-launched AUVs, particularly in high-speed conditions, and reported that the axial and radial accelerations during the early stage of water entry under different conditions provide essential data for understanding the dynamic behavior of air-launched AUVs.

Shi et al. (2019b) investigated hydrodynamic effects during water entry due to the shell's elastic deformation, affecting their load response, also the factors affecting head shape, shell thickness, water-entry velocity, and angle, influence the acceleration, pressure, stress, and structural deformation of the AUV by comparing with experimental drop-test data. Shi et al. (2019a) studied the effect of impact forces and cavity formation on the load dynamics and trajectory stability by developing a numerical model and simulating the cavity shape and impact load characteristics of a high-speed water-entry AUV. The simulation results are validated by comparison with experimental data, showing strong agreement and confirming the accuracy of the numerical algorithm. Pan and Guo (2013) focused on developing an optimized wing design for AL-AUV performance using traditional REMUS torpedo-like autonomous underwater vehicles and producing high-altitude air-launched autonomous underwater vehicles. Zhang et al. (2021) investigated the change in AUV velocity during launch from underwater vehicle tubes and reported that the AUV accelerates as it approaches the second seal ring, but its momentum decreases when the pressure difference between the front and rear end of the vehicle becomes minimal. Wang (2012) examined the water-entry impact of air-launched autonomous underwater vehicles which operates as a time-dependent and strongly nonlinear fluid-structure interaction phenomenon. The study emphasizes the importance of a precise numerical modeling technique for studying how water-entry impact loads function and how fluid interactions affect vehicle responses during this process. The research results provide significant knowledge for designing structures and analyzing hydro ballistic characteristics in air-launched AUVs.

Chen (2019) studied the dynamics of water entry impact affecting autonomous underwater hovering vehicles (AUH). The research findings stress the necessity to comprehend non-linear and asymmetrical water entry forces alongside their application in designing future AUHs while determining airborne-launched vehicle operational limits. Wu et al. (2022) investigated the water entry of air-launched underwater gliders under wave conditions and determined the effects of entry points and attack angles and entry angles on impact forces, thus guiding the glider design. Chaudhry et al. (2020) investigated the water entry process of air-launched AUVs using a penalty coupling technique for the finite element method and arbitrary Lagrange-Euler formulation (FEM-ALE). The research reveals important details about the AUV design structure and the selection of optimal water entry parameters. Qi et al. (2016) analyzed the water entry impact of an air-launched AUVs, showing that both entry angle and initial speed directly influence the impact loads. This research offers significant knowledge about AUV structural development and the identification

of the best launch parameters. Zhang et al. (2017) developed a study on the water entry process of AUV through volume of fluid (VOF) and overset mesh technology to determine pressure distributions and impact loads accurately and reported that entry angles and initial velocity data are important to analyse for future air-launched AUV designs.

The authors expressed the work done so far in the above section. The rest of this paper is organized as follows In section 2, the problem description illustrating the method and methodology along with the governing equation, computational domain, mesh generation, boundary conditions, and numerical validation will be presented. In sections 3 and 4, results and discussions will be presented, and finally, in section 4, the conclusions of the work will be presented.

2 Methods and methodology

2.1 AUV structure

The AUV discussed is an axisymmetric body with a four-numbered NACA 0012 profile having a mass of 74.77 kg. The AUV is considered rigid with a constant mass and shape. Only gravity accelerates the AUV during free fall. Aerodynamic drag is neglected for simplicity. Impact velocities are estimated based on free fall height. There are three main hull forms used for AUVs: Myring's Profile, Jackson's Profile, and Gertler's Series 58 Profile. Although the equations for these profiles differ, they essentially represent similar shapes with minor variations (Sener and Aksu, 2022). Figure 1 represents the shape of the AUV. The AUV geometry is typically divided into three sections: the nose, the body, and the tail, all designed using Myring's equations (Myring, 1976). To design the nose and tail shapes, Equations (2) are employed.

$$R_1(x_1) = \frac{1}{2}\left[1 - \left(\frac{x_1 - a}{a}\right)^2\right]^{\frac{1}{n}} \tag{1}$$

$$R_2(x_2) = \frac{1}{2}D_{\max} - \left[\frac{3D_{\max}}{2c^2} - \frac{\tan\theta}{c}\right]x_2^2 + \left[\frac{D_{\max}}{c^3} - \frac{\tan\theta}{c^2}\right]x_2^3 \tag{2}$$

where D represents the maximum diameter of the model; a represents the length of the nose; x_1 represents the location of the nose tip; c represents the length of the tail; θ represents the tail half angle in degrees; n represents the Myring body parameter; L represents the length of the AUV. The dimensions of the profile are illustrated in Table 1. The control surface is NACA 0012 having a mean span and chord length of 0.060 525 m and 0.25 m respectively. The study explores the hydrodynamic performance of AUV, focusing on factors like water entry angle, impact velocity, and impact pressure.

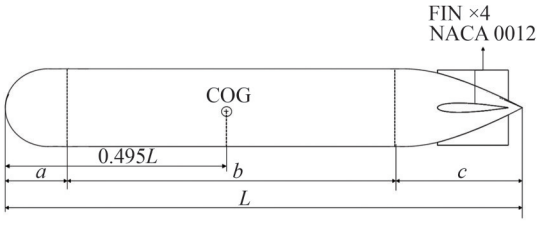

Figure 1 Shape of the AUV

Table 1 Dimensional parameters of AUV

Description	Value
Nose length (m)	0.15
Hull length (m)	1.256 25
Tail length (m)	0.418 75
Maximum diameter (m)	0.25
Tail half angle (°)	25
Myring body parameter	2
Length of AUV (m)	1.825

2.2 Governing equations

Considering the influence of gravity, a series of transient three-dimensional CFD simulations were performed to evaluate the performance of the AUV. The ANSYS Fluent CFD software was used to solve the Reynolds-averaged Navier-Stokes (RANS) equations with a SIMPLE pressure-velocity coupling scheme. The governing equations include the continuity equation and the momentum equation, which are presented in Equations (3) and (4), respectively.

$$\frac{\partial \rho}{\partial t} + \frac{\partial \rho \overline{v_i}}{\partial x_i} = 0 \tag{3}$$

$$\frac{\partial}{\partial t}(\rho \overline{v_i}) + \frac{\partial}{\partial x_i}(\rho \overline{v_i}\overline{v_j}) = -\frac{\partial p}{\partial x_i} + \frac{\partial}{\partial x_j}\left[\mu\left(\frac{\partial \overline{v_i}}{\partial x_j} + \frac{\partial \overline{v_j}}{\partial x_i} - \frac{2}{3}\delta_{ij}\frac{\partial v_l}{\partial x_l}\right)\right] - \frac{\partial}{\partial x_j}\left(\rho \overline{v_i' v_j'}\right) + F_i \tag{4}$$

The equations represent the velocity components, p denotes the pressure, F_i represents the external body force components, and μ denotes the dynamic viscosity. The velocity is the combination of the time-averaged value $\overline{v_i}$ and the fluctuation v_i'.

The shear stress transport (SST) k-ω turbulence model was chosen to handle the turbulence terms in the RANS equations. The SST variant combines features of both the k-ε and k-ω models, offering accurate predictions across various flow scenarios, including near-wall regions, free shear layers, and adverse pressure gradients. The model computes the turbulent kinetic energy, k, and the specific dissipation rate, ω, using the Equations (5) and (6).

$$\frac{\partial}{\partial t}(\rho k)+\frac{\partial}{\partial x_i}(\rho k v_i)=\frac{\partial}{\partial x_j}\left[\tau_k\frac{\partial k}{\partial x_j}\right]+G_k-Y_k+S_k \quad (5)$$

$$\frac{\partial}{\partial t}(\rho\omega)+\frac{\partial}{\partial x_i}(\rho\omega v_i)=\frac{\partial}{\partial x_j}\left[\tau_\omega\frac{\partial k}{\partial x_j}\right]+G_\omega-Y_\omega+D_\omega+S_\omega \quad (6)$$

where G_k and G_ω represent the generation of k and ω resulting from turbulent mean-velocity gradients, respectively, τ_k and τ_ω signify effective diffusivity, while Y_k and Y_ω represent the dissipation of k and ω due to turbulence, D_ω represents the cross-diffusion term, and S_k and S_ω are user-defined source terms.

The VOF method is used to predict fluid behavior during transient flows, effectively representing the sharp interface between air and water surfaces caused by wave propagation. This method relies on the concept of air-water mixture velocity, which involves tracking the volume fraction of each fluid phase within the computational domain, as shown in Equation (7).

$$v_i=\sigma v_i^a+(1-\sigma)v_i^w \quad (7)$$

where σ represents the volume, fraction equals 1 when fully occupied by air, v_i^a denotes the velocity for the phase of air, and v_i^w denotes the velocity for the phase of water.

2.3 Computational domain and mesh generation

Figure 2 illustrates the computational domain of the work. This vertical domain spans a length of 360D; the upper portion contains air, while the lower portion contains water, at a height corresponding to 20D and 400D, respectively. The AUV is positioned exactly at the center at a distance corresponding to the desired height. The boundary conditions include uniform pressure as an inlet, pressure outlet as an outlet, no-slip wall conditions on AUV surfaces, and smooth wall conditions on the remaining surfaces. Overset mesh technology is utilized, enabling the transfer of flow field data between the subdomains through interpolation, as shown in Figure 3. A mesh discretization is performed to assess the impact of grid resolution corresponding to the average value of skewness with different grid cells, thereby calculating the value of y^+ as shown in Equation (8). It is a dimensionless parameter used for solving the viscous sublayer in capturing the boundary layer flow. It is calculated by the following equation

$$y^+=\frac{\Delta y_1}{\frac{\mu}{\sqrt{\rho\,\tau_w}}} \quad (8)$$

where Δy_1 is the cell layer thickness measured vertically to the wall, μ is the dynamic viscosity of the fluid, ρ is the density of the fluid, and τ_w is the shear stress in the wall. The results indicate that grids having 7.2 million and 6.7 million cells produce similar outcomes. Consequently, the 6.7 million element grid ($y^+ < 30$) is chosen for subsequent simulations, as shown in Figure 4.

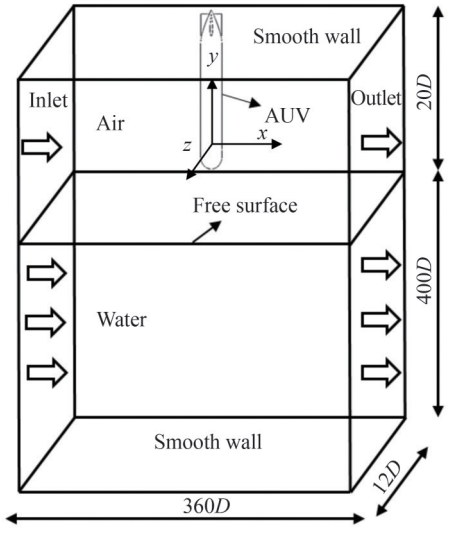

Figure 2 Schematic illustration of computational domain and boundary conditions

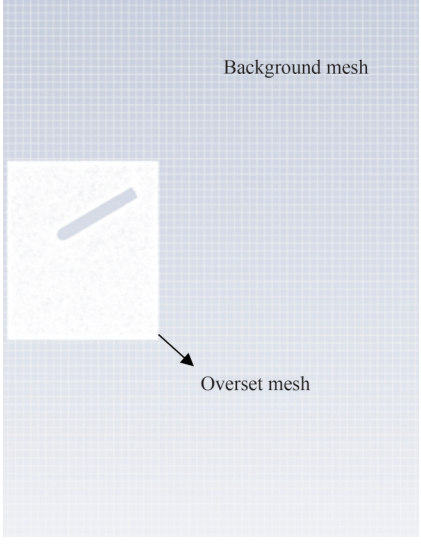

Figure 3 Mesh generation on a plane section

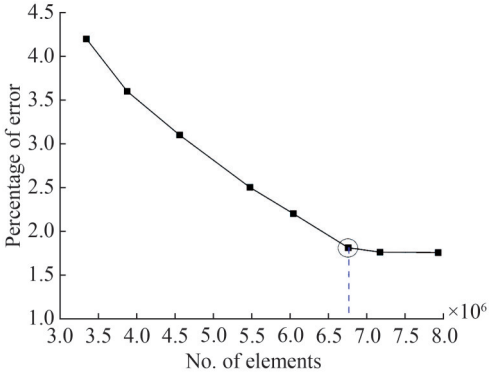

Figure 4 Grid discretization study

2.4 Numerical method verification and validation

In CFD calculations, verification and validation processes are essential to evaluate the reliability and accuracy of numerical results (ITTC, 2017). Verification can be divided into code and solution verification. Code verification checks whether the CFD software accurately solves the governing equations, while solution verification calculates numerical uncertainties (U_N) of the computed variables. This study did not include code verification as simulations were performed using ANSYS Fluent, where codes undergo verification before each release. Numerical uncertainties are estimated by multiplying the numerical error by a safety factor. The numerical error consists of three parts i.e., round-off error, iterative error, and discretization error (Hoekstra, 2016; Eça et al., 2010). Round-off error is minimized due to the use of double precision during setup conditions. The iterative error is the difference between the actual numerical solution and the solution obtained after an infinite number of iterations. Discretization error is the difference between the exact solution of the continuous problem and the solution of the discretized problem. It depends on factors such as the size of the intervals (or grid size) and the order of the numerical method used; generally, reducing the interval size or using higher-order methods reduces the discretization error. However, this reduction often comes at the cost of increased computational resources. It is stated that numerical uncertainties (U_N) are primarily affected by grid discretization. Validation is defined as a process for assessing numerical results by using benchmark experimental data. This comparison involves calculating the difference between simulation and experimental data, known as comparison error (E), by using Equation (9).

$$E = D - N \tag{9}$$

$$\text{Relative error} = (E/D) \times 100 \tag{10}$$

The validation of the numerical results is done by calculating the impact acceleration of the AUV. It is calculated for a water entry angle of 60° by validating the experimental data conducted by Chaudhry et al. (2021) as shown in Figure 5. The results are aligned closely with the experimental data by using Equation (10) with a relative error of 4.57% at 9.75 ms. It is observed that impact acceleration increases as the entry velocity increases for a given entry angle and also increases with a higher entry angle at a constant entry velocity. Impact acceleration is further processed in terms of impact coefficient (C_s) for different entry angles and entry velocities. The impact coefficient (C_s) is a dimensionless parameter that characterizes the severity of the impact load experienced by an AUV during water entry. It helps to assess the magnitude of hydrodynamic forces acting on the AUV at the moment of water entry. A higher value indicates a more severe impact, which could influence the AUV's structural and operational performance. The impact coefficient (C_s) was determined by using Equation (11).

$$C_s = \frac{2F_{\text{imp}}}{\rho \pi R^2 v^2} \tag{11}$$

where F_{imp} is the total impact load during water entry, ρ is the fluid density, R is the AUV diameter, and v is the entry velocity of AUV. Figure 6 illustrates a linear relationship between the impact coefficient and impact velocity during the process of water entry. Additionally, it is observed that the impact acceleration of the AUV follows a second-order relationship with the velocity of water entry. Figure 7 further demonstrates that the impact coefficient of the AUV is proportional to the square of the entry angle. The convergence criterion suggested by the ANSYS Fluent is used in this study with a time step size of 0.004. The simulation was carried out for 5 s.

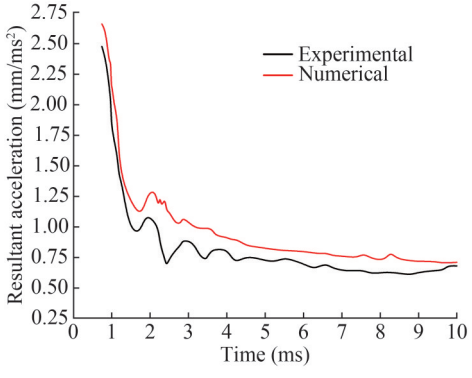

Figure 5 Validation of acceleration

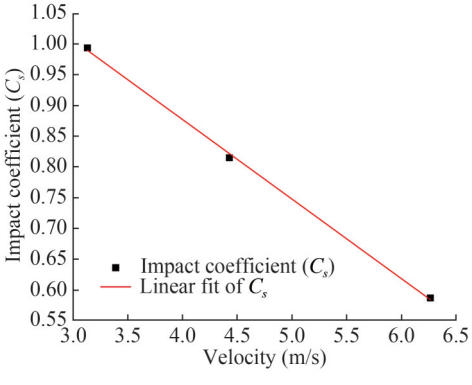

Figure 6 Impact coefficient for different velocities

3 Results

3.1 General flow characteristics

The general flow characteristics around an AUV during water entry at various angles exhibit distinct patterns due to variations in flow separation. These flow characteristics influence the resultant forces, stability and trajectory of an

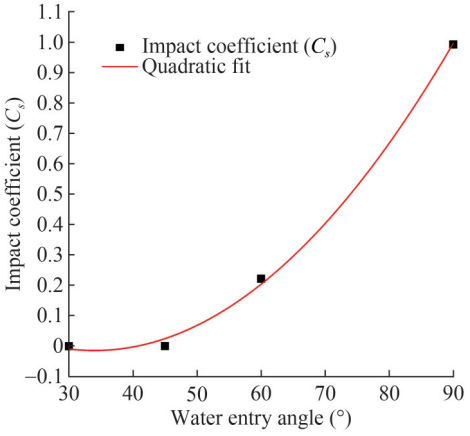

Figure 7 Impact coefficient for various water entry angles

AUV. For an entry angle of 30°, the AUV experiences moderate drag upon entry, with more horizontal force pushing it forward rather than deep. The AUV undergoes significant surface drag and resistance, limiting its depth of penetration. Velocity magnitudes are lower in the vertical direction due to the shallow entry, with a stronger horizontal component dominating the flow. Stability is more challenging under these conditions, with a high chance of pitching during impact. The acceleration is also less intense compared to steeper entry angles due to the reduced drag force and a significant component of the velocity vector aligning in the horizontal direction. The body maintains a more gradual change in acceleration because of the smaller vertical force contributions. The body requires a longer time to stabilize, indicating that horizontal motion delays the establishment of steady-state forces. The AUV experiences a smooth entry with a controlled trajectory, providing a stable descent corresponding to an entry angle of 45°. This angle and height combination ensures a predictable path with minimal pitch, making it ideal for shallow to moderate-depth entry. Velocity vectors show a balanced distribution between horizontal and vertical components. It is observed that a stable descent with a slight increase in pitching tendency is due to increased horizontal force. This condition allows the AUV to achieve greater depth while maintaining a stable trajectory. For a steeper entry angle of 60°, the AUV experiences a stable descent due to the dominant vertical force. The domination of the vertical velocity component leads to deeper and faster-moving water in the surroundings of the AUV. With the presence of minimal horizontal force, the AUV moves in a straight trajectory, making it ideal for quick and controlled vertical entry. Due to the presence of surface tension and higher frontal area during the impact, there is a consistent decrease in resultant acceleration, which takes more time for the AUV to stabilize. At steeper entry angles, a larger portion of the velocity vector is aligned with the vertical direction, resulting in the hydrodynamic drag acting more effectively to decelerate the vehicle. The acceleration experienced by the AUV is primarily due to the combined effects of drag force and buoyancy, which oppose the motion along the AUV's trajectory. Since the AUV follows an inclined path during water entry, the resistive forces act along the AUV trajectory, and the position of CG of the AUV tends to change with respect to time, as shown in Table 2. For a vertical fall of 90°, AUV experiences a direct, stable descent with minimal deviation. The AUV maintains its straight trajectory due to high stability, providing a controlled path into the water. This is due to the dominant vertical motion, resulting in stronger drag and buoyancy forces countering the motion. At 90°, the acceleration reaches its peak quickly, indicating that the resultant forces dominate immediately after entry. The NACA 0012 airfoil present at the tail of the AUV enhances the stability by generating hydrodynamic forces to counteract the deviations caused by asymmetric water impact thereby reducing the risk of tumbling and improving directional stability. Figure 8 represents the acceleration behavior for different entry angles of 30°, 45°, 60°, and 90° corresponding to various entry velocities of 3.132 m/s, 4.429 m/s, and 6.264 m/s. From the analysis, it was seen that the resultant acceleration is more significant at higher entry angles of 90° compared to lower angles of 30°. The resultant acceleration increases sharply at the beginning and then stabilizes as time progresses, suggesting that the impact force is highest upon water entry and diminishes as the AUV continues its descent. As the velocity increases, the acceleration becomes distinct across all entry angles following a consistent trend thereby a gradual decrease as the AUV enters into water. At 3.132 m/s, the acceleration is relatively less severe, and all the curves follow a smooth decreasing trend. At 4.429 m/s, the trend remains similar but with higher accelerations, particularly for steeper entry angles of 60° and 90°. As the water entry angle increases, the resultant acceleration also increases with its highest value at a velocity of 6.264 m/s corresponding to an entry angle of 90°.

Figure 9 represents the volume fraction contours of an AUV corresponding to different angles of water entry. It is observed that the time taken for the AUV to impact the water surface decreases with increasing entry angles, with durations of 0.4 s for 30°, 0.32 s for 45°, 0.20 s for 60°, and 0.12 s for 90°. This is due to the velocity distribution between the horizontal and vertical components. The horizontal component is more significant, as the AUV follows a longer diagonal path before reaching the water surface, increasing the time required. As the entry angle increases, the vertical component of velocity becomes dominant. At 90°, the velocity is entirely vertical, leading to the shortest travel time to the surface. Secondly, gravity accelerates the vertical motion of the AUV, which induces a higher vertical velocity component, resulting in faster acceleration and further reducing the impact time. For an entry angle of 30°, there is minimal disturbance at the water surface, and

Table 2 Position of CG corresponding to water entry angle of 60° with a velocity of 4.429 m/s

Time (s)	*X*-axis (m)	*Y*–axis (m)
0.000000	0.456250	1.790000
0.004000	0.448562	1.776680
0.008000	0.440822	1.763280
0.012000	0.433015	1.749760
0.016000	0.425140	1.736120
0.020000	0.417197	1.722360
0.024000	0.409185	1.708480
0.028000	0.401106	1.694490
0.032000	0.392959	1.680380
0.036000	0.384744	1.666150
0.040000	0.376461	1.651810
0.044000	0.368110	1.637340
0.048000	0.359691	1.622760
0.052000	0.351204	1.608060

the transition zone is smooth and narrow. The AUV also experiences a shallow entry, with reduced vertical penetration into the water. Moderate disturbance has been observed at the water-air interface for an entry angle of 45°. The AUV begins to penetrate deeper, creating a larger wake. For steeper entry angles of 60° and 90°, there is Significant disruption of the water surface. The transition zone becomes broader, indicating more mixing between water and air. The AUV penetrates deeper, with a noticeable wake and splashing. Shallow entry angles of 30° and 45° are more energy-efficient due to lower drag and minimal surface disruption. Steeper entry angles of 60° and 90° provide better penetration into the water, but as a result, there is an increase in drag and turbulence characteristics.

3.2 Influence of water entry angle

The water entry angle significantly influences the dynamics of an AUV impacting the water surface, as different angles affect the generation of splash, impact forces, trajectory, stability, and depth of penetration. With a shallow entry angle of 30°, the AUV experiences relatively lower vertical impact forces because a larger portion of the initial momentum is directed horizontally rather than vertically leading to the formation of an elongated splash and surface disturbance, with a significant amount of kinetic energy dissipated over the surface, creating a longer wake. The AUV also experiences less stability upon entry as it moves over the water surface, potentially leading to instability due to pitching motion. Its gradual transition into water leads to lower impact pressures, minimizing shock formation and ensuring a smoother pressure distribution along its surface. Additionally, at higher velocities, the AUV exhibits an increased tendency for the ricochet effect. At an angle of

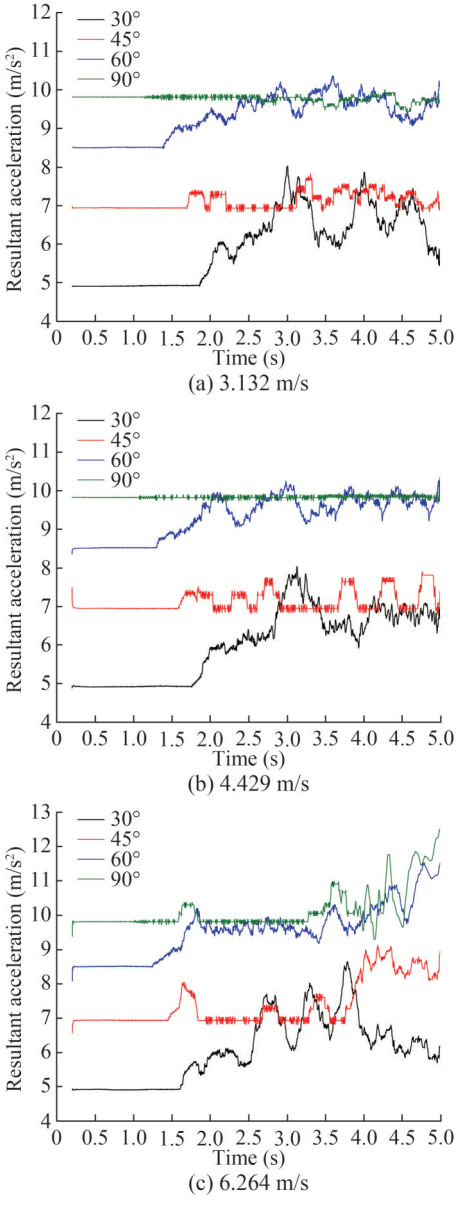

Figure 8 Represents the resultant acceleration of the AUV at different velocities

45°, the AUV experiences a balance between vertical and horizontal impact forces, leading to moderate force distribution across both components, which helps in balancing the load on the AUV's structure. The splash and surface disturbance are typically symmetrical and moderate in size. The AUV's trajectory is relatively stable, with a balanced descent that minimizes the risk of excessive pitch. The 45° angle offers an optimal balance for maintaining control and stability during entry. This configuration allows for effective momentum transfer without excessive surface disruption, making it ideal for entry. As a result, it is commonly employed to minimize the forces while maintaining overall stability. From the analysis of the results, it was also found that for an entry angle of 45°, the averaged value

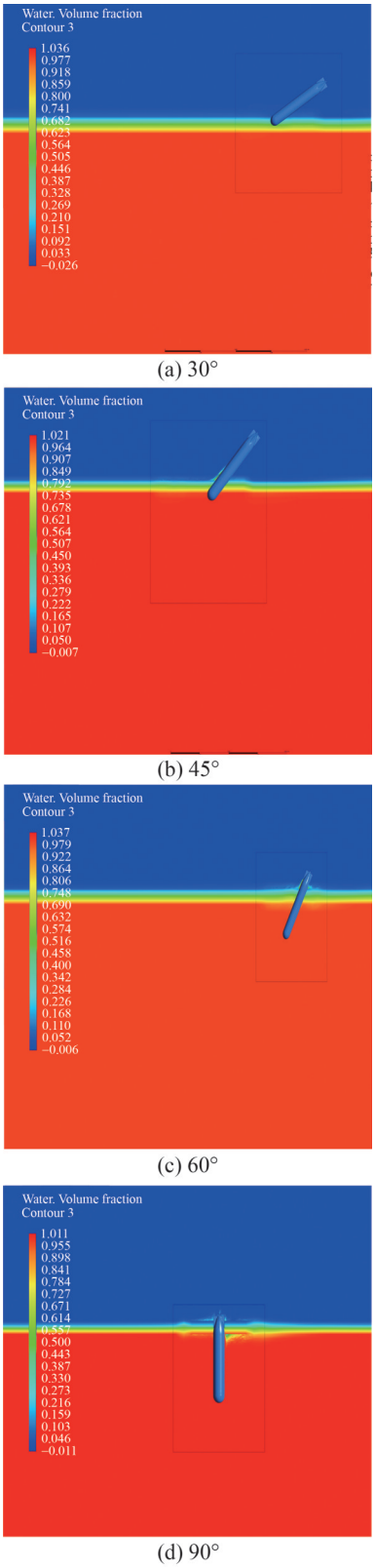

Figure 9 Phase contours of AUV during its descent for $v = 3.132$ m/s at $t = 0.4$ s

of resultant forces is 31.4% higher than that obtained for a shallow angle of 30° corresponding to the velocity of 3.132 m/s. A steeper angle of 60° results in higher impact force and subjects the AUV to greater stress upon entry, offering a balance between vertical penetration and stability, making it a practical choice for controlled descent. The force distribution is more concentrated in creating a more intense, downward impact resulting in the generation of a narrower splash but more forceful, with water jetting upwards and minimal horizontal spread. This is due to the greater downward momentum compared to shallow angles. A 60° entry generally enhances stability as the AUV's motion is more controlled vertically. However, the high impact force causes pitching, thereby providing quicker vertical descent, allowing the AUV to achieve greater depths in a shorter time. This reduces the ricochet effect but increases the impact forces. Additionally, the steeper entry angles result in greater hydrodynamic resistance compared to shallower angles. At a vertical 90° entry angle, the AUV experiences maximum vertical impact force creating the entire momentum downwards, thereby creating a strong impact over the water surface. The splash is highly vertical and compact, with a minimal horizontal spread. This entry is ideal for minimizing the horizontal area affected by the splash but is highly energetic, thereby creating a tall column of water upon impact. A vertical entry ensures a straight descent, maximizing the stability and minimizing the pitch. Maximum impact pressure at the point of water contact. During this entry angle, this steep impact significantly raises the chances of cavitation and shock formation, leading to an increase in flow separation and turbulence, which affect the stability and hydrodynamic performance. Higher entry angles, such as 60° and 90°, experience greater forces due to a more direct impact with the water surface, leading to higher resistance, as shown in Figure 10. The forces acting on the AUV during water entry are highly sensitive to the entry angle. Steeper angles lead to a greater amount of resultant force, making them ideal for vertical penetration and stability but with higher structural demands. Shallow entry angles reduce the amount of resultant force, favoring efficient and extended horizontal trajectories. It is observed that the selection of the entry angle should depend on the specific operational requirements, stability, and energy efficiency.

3.3 Influence of impact velocity

In this section, the influence of three different impact velocities (3.132 m/s, 4.429 m/s and 6.264 m/s) at a water entry angle of 60° on the behavior of an AUV is analyzed in terms of key parameters such as impact forces, pressures, stability, and depth of penetration. It is observed that when an AUV enters the water, it interacts with a virtual mass of fluid, known as added mass, which increases the effective inertia of the vehicle. For a low velocity of 3.132 m/s, the AUV experiences a controlled entry with mild structural loading, which results in reduced drag during initial descent due to relatively low vertical impact forces to

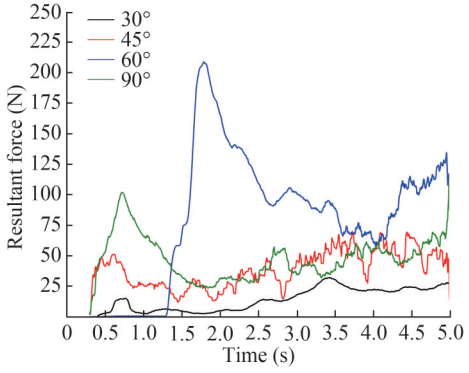

Figure 10 Represents the resultant force corresponding to a velocity of 4.429 m/s

moderate kinetic energy during impact. The AUV maintains a stable trajectory due to the moderate impact force and minimum lateral disturbances, ensuring consistent vertical descent with minimal pitch. The AUV achieves a moderate depth of penetration. The velocity field is highly elongated, with significant horizontal spreading of water particles. Figure 11 represents the forces corresponding to different velocities for an entry angle of 45°. For a moderate velocity of 4.429 m/s, the AUV experiences a large number of forces that are sufficient to cause structural stress at the impact point, though stability during descent remains intact. Stability remains robust but with an increased risk of minor pitch deviations due to higher forces acting on the AUV. The entry angle ensures a relatively smooth descent. The depth of penetration increases due to higher momentum, making it suitable for medium-depth operations. The descent remains controlled but is faster than at lower velocities. From the analysis of the results, it is observed that there is an increase in the average resultant force due to an increase in resistance and momentum transfer to the surrounding water. For a high velocity of 6.264 m/s, the AUV experiences significantly high vertical impact force, with the AUV experiencing substantial momentum transfer to the water. These high forces challenge the structural area at the nose to prevent damage. Stability is more challenged due to higher dynamic forces and pressures. The risk of oscillatory motion increases slightly, but the steeper entry angle reduces significant deviations. The maximum depth of penetration is observed among the three scenarios. The added mass effect is more pronounced at 6.264 m/s, where the pressure field around the AUV is highly concentrated, which leads to a rise in average force. For shallow entry angles, the contours exhibit gradual transitions, with a wide distribution of velocity near the surface as the water flows outward. For steeper entry angles, the contours are relatively narrow, indicating focused energy transfer into the water. The velocity field is the most symmetric, with vertical velocities peaking directly below the entry point. Minimal horizontal spreading is observed, with velocity magnitudes quickly reducing laterally but extending significantly downward. At lower speeds, the water entry process is smoother, with lower impact forces and minimal chances of cavitation. At moderate speeds, the pressure gradients intensify, increasing hydrodynamic resistance and impact forces. At high speeds of 6.264 m/s, strong pressure variations induce cavitation, increasing drag and energy dissipation.

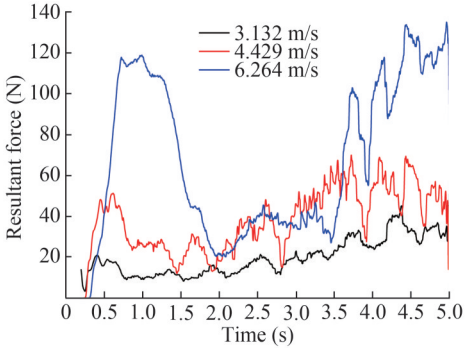

Figure 11 Represents the resultant force corresponding to different velocities for an entry angle of 45°

Figure 12 represents the velocity contours of the AUV during its descent for various angles of water entry. From the analysis, it is observed that for an entry angle of 30°, the flow separates smoothly along the body with minimal wake formation downstream. The velocities are high around the leading edges, where the flow interacts with the AUV, leading to the formation of the narrow wake. For an entry angle of 45°, a more noticeable amount of flow separation takes place, resulting in a slightly wider wake. The velocity gradient tends to increase at the leading edge and midsection of the AUV. For 60°, Flow separation becomes more pronounced, leading to a significant increase in wake size. High-velocity zones shift further along the leading edge and concentrate towards the midsection. For 90°, the blunt orientation of the AUV results in a large stagnation region at the front. Significant flow separation occurs at the edges, forming a large recirculation zone in the wake. The wake is the widest here, with noticeable low-velocity regions behind the AUV. High velocities near the leading edge of the AUV at smaller angles indicate flow acceleration as water moves around the streamlined body. Increasing the water entry angle results in larger wake regions with more recirculation and lower velocities. As the entry angle increases, the wider wake and stronger separation suggest higher drag forces acting over the surface of the AUV. This highlights the importance of optimizing the entry angle based on mission-specific requirements to balance stability, impact forces, and desired underwater trajectory.

3.4 Influence of impact pressure

When it comes to the entry of an AUV into the water, impact pressure acts as one of the crucial parameters that

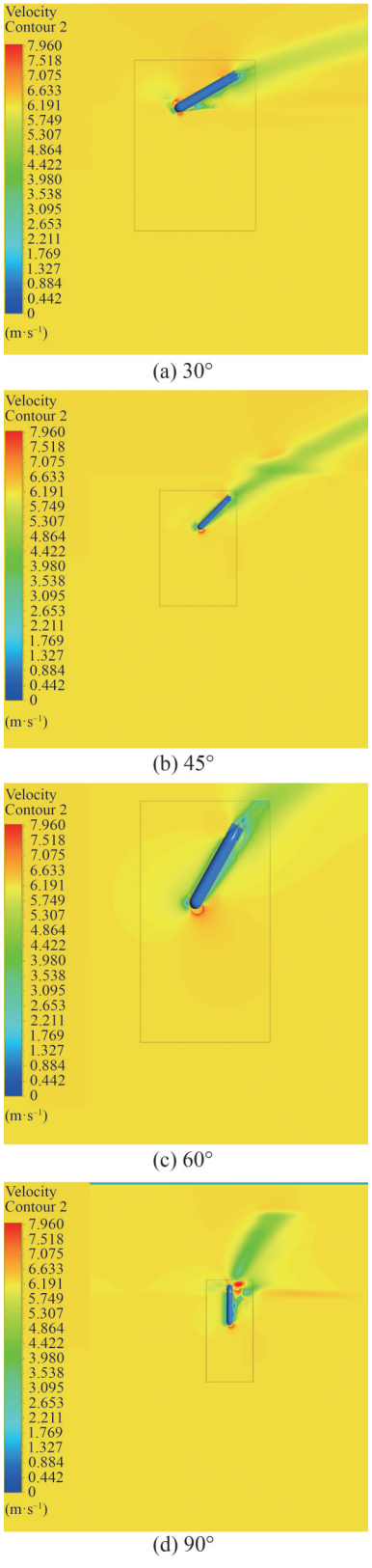

Figure 12 Velocity contours of AUV during its descent to various water entry angles for a velocity of 6.264 m/s at $t = 0.8$ s

affect the hydrodynamic forces. Impact Pressure is always generated and depends on the angle of entry, which has the rotation index. For an entry angle of 30°, the AUV gets the minimal impact pressure as the normal component of the velocity is minimal. A reduction in the angle results in less force being effective on the vehicle, which means that the chances of being hit on the inside structure decrease. With an entry angle of 45°, impact pressure increases compared to 30°. This is due to the larger normal velocity component at 45°, which is halfway between purely horizontal and vertical entry. For an entry angle of 60°, Impact pressure is further increased as the vertical component of the velocity vector is completely aligned normal to the water surface. This angle introduces a significant amount of energy dissipation, improving stability but increasing structural stress. The AUV encounters the greatest hydrodynamic resistance, leading to maximum energy dissipation and structural impact. As the angle increases from 30° to 90°, the normal velocity component increases, resulting in a quadratic rise in impact pressure. Steeper angles impose higher hydrodynamic forces, requiring the AUV to have enhanced structural strength to withstand the pressure. Lower angles of 30° and 45° distribute the forces over a longer trajectory, reducing peak pressures and structural stress but increasing potential horizontal displacement. Higher entry angles dissipate more kinetic energy rapidly upon impact, leading to a greater reduction in velocity. Figure 13 represents the impact pressure on the AUV during its descent. It is observed that with an increase in velocity and entry angle, the impact pressure tends to increase.

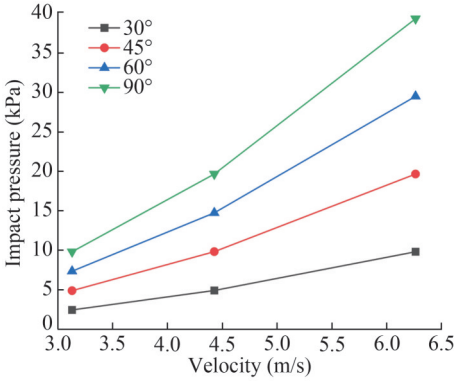

Figure 13 Represents the impact pressure on the AUV during its descent

Figure 14 shows the pressure contours of the AUV during its descent for an entry angle of 60°. It is observed that at a velocity of 3.132 m/s, high-pressure zones are observed at the leading edge and the aft-most region of the AUV. Pressure decreases smoothly along the surface as water accelerates over the AUV. A low-pressure region exists downstream of the AUV due to flow separation. The pressure gradient is low due to the lower velocity. The pressure distribution shows moderate variations, with relatively lower peak pressures at the impact zones. The pressure gradients suggest a smooth transition from air to water, with

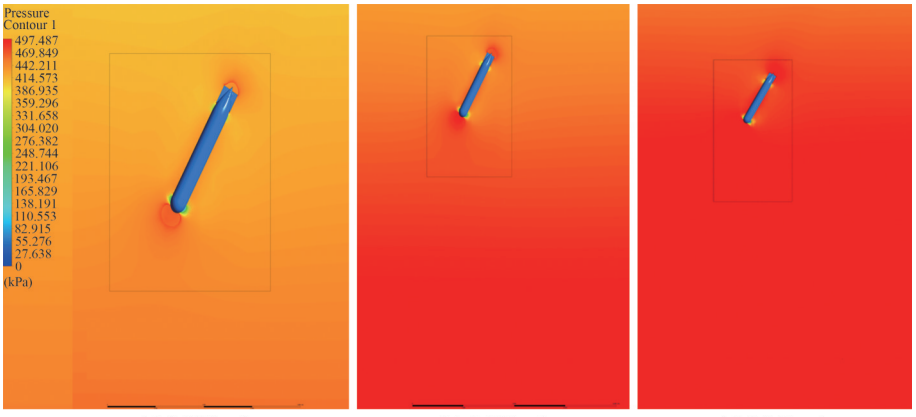

(a) 3.132 m/s (b) 4.429 m/s (c) 6.264 m/s

Figure 14 Pressure contours of AUV during its descent for an entry angle of 60° at $t = 3.2$ s

less intense shock formation. The flow is less dynamic compared to higher speeds. At a velocity of 4.429 m/s, the high-pressure zone at the leading edge becomes more intense, covering a slightly larger area. A stronger low-pressure region develops on the body, especially along the sides, as water accelerates faster over the surface. The wake behind the AUV becomes more prominent, indicating increased flow separation. The pressure gradient increases, causing stronger suction forces along the body. Due to the increase in impact force, more pronounced pressure peaks have been observed at the entry points, indicating a higher resistance, which enhances the local pressure variations around the AUV. At 6.264 m/s, Maximum pressure (~497.487 kPa) occurs at the stagnation points with an intensified low-pressure region along the sides of the body. The wake grows significantly, with the lowest pressures observed immediately downstream of the AUV. The pressure difference between the front and the aft region increases, indicating a greater amount of hydrodynamic forces. At this high velocity, the pressure distribution highlights significant pressure drag and flow separation effects. It is observed that Shear stress is highest at the points of high-velocity gradients, such as the sides of the AUV where the flow accelerates rapidly. Shear stress increases with an increase in velocity, leading to higher skin friction at 6.264 m/s compared to the lower velocities. Flow separation in the wake region at higher speeds results in low shear stress due to reduced interaction between the body and the flow.

4 Conclusions

Based on the numerical investigations conducted on the oblique water entry dynamics of an AUV impacting the water surface under varying entry angles of 30°, 45°, 60°, and 90° and impact velocity, the following conclusions are drawn:

1) Increasing the free-fall height significantly increases the impact velocity, which results in high impact forces upon entry. The forces experienced at the leading edge of the hydrofoils remain mostly unaffected as the AUV descends into water.

2) For Steeper entry angles, AUVs had a better chance of getting the desired depth. This means that there is a greater chance of minimizing the horizontal force interactions. Shallower entry angles cause an even distribution, but great impact force is experienced at the bow end of the AUV.

3) At shallower entry angles of 30° and 45°, the pressure during the impact is more evenly spread across the underside of the AUV, lowering peak pressures but increasing the instability due to pitching.

4) Steeper entry angles of 60° and 90° allow for more stable and vertical entry since the AUV experiences less lateral deviation and minimal pitch, resulting in a controlled and predictable descent.

5) Operating at shallow entry angles results in greater oscillations that induce the increase of surface skimming or bouncing effects, particularly for higher heights.

6) Steeper entry angles enable more efficient depth of penetration, with minimal horizontal displacement and a rapid descent path. The AUV achieves maximum depth quickly, which is advantageous for applications requiring deep and immediate submersion.

7) At shallow entry angles, the AUV has a longer horizontal trajectory and reduced depth of penetration due to the greater horizontal impact force. This limits the effectiveness of the AUV for missions that require deeper water operations immediately after entry.

These findings are particularly relevant for the design and operational planning of AUVs deployed in missions requiring precise control over entry dynamics. These include naval operations, underwater surveillance, environmental monitoring, and deep-sea exploration, where optimizing impact forces, stability, and depth control is crucial. By analyzing different entry angles and impact velocities, our study provides valuable guidelines for selecting optimal entry conditions to enhance AUV performance. In future scope, how cavitation bubble formation and collapse play a crucial

role in governing the flow dynamics, pressure distribution, and potential effects on the AUV can be analyzed.

Nomenclature

a	Length of the nose
b	Length of the cylinder
c	Length of the tail
C_s	Impact coefficient
D	Experimental data
$D_{\max}$	Maximum diameter of the model
E	Comparison error
F_{imp}	Total impact load during water entry
F_i	External body force components
L	Length of the AUV
n	Myring body parameter
N	Numerical results
R	AUV diameter
U_N	Numerical uncertainties
v	Water entry velocity of AUV
v_i	Velocity components
x_1	Location of the nose tip
x_2	Location of the tail tip
y^+	Non-dimensionless parameter
Δy_1	Cell layer thickness measured vertically to the wall
θ	Tail half angle in degrees
ρ	Fluid density
μ	Dynamic viscosity of the fluid

Competing interest The authors have no competing interests to declare that are relevant to the content of this article.

References

Amiri MM, Sphaier SH, Vitola MA, Esperança PT (2019) URANS investigation of the interaction between the free surface and a shallowly submerged underwater vehicle at steady drift. Applied Ocean Research 84: 192-205. https://doi.org/10.1016/j.apor.2019.01.012

Chaudhry AZ, Shi Y, Pan G (2020) Study on the oblique water entry impact performance of AUV under different launch conditions based on coupled FEM-ALE method. AIP Advances 10(11): 115020. https://doi.org/10.1063/5.0025741

Chaudhry AZ, Shi Y, Pan G, Liu G (2021) Mechanical characterization of flat faced deformable AUV during water entry impact considering the hydroelastic effects. Applied Ocean Research 115(3): 102849. https://doi.org/10.1016/j.apor.2021.102849

Chen T, Huang W, Zhang W, Qi Y, Guo Z (2019) Experimental investigation on trajectory stability of high-speed water entry projectiles. Ocean Engineering 175: 16-24. https://doi.org/10.1016/j.oceaneng.2019.02.021

Chen Y, Chen X, Li J, Gong Z, Lu C (2017) Large eddy simulation and investigation on the flow structure of the cascading cavitation shedding regime around 3D twisted hydrofoil. Ocean Engineering 129: 1-19. https://doi.org/10.1016/j.oceaneng.2016.11.012

Choe Y, Kim C (2022) Computational investigation on ventilated supercavitating flows and its hydrodynamic characteristics around a high-speed underwater vehicle. Ocean Engineering 249: 110865. https://doi.org/10.1016/j.oceaneng.2022.110865

Eça L, Vaz G, Hoekstra M (2010) A verification and validation exercise for the flow over a backward facing step. Eccomas CFD 2010: 14-17

Eça L, Vaz G, Hoekstra M (2010) Code verification, solution verification and validation in RANS solvers. Proceedings of the ASME 2010 29th International Conference on Ocean, Offshore and Arctic Engineering, Shanghai, China, 597-605. https://doi.org/10.1115/OMAE2010-20338

Fronzeo MA, Kinzel M, Lindau JW (2019) An assessment of pressure variations in artificially ventilated cavities. Ocean Engineering 177: 85-96. https://doi.org/10.1016/j.oceaneng.2019.02.045

Gaudet S (1998) Numerical simulation of circular disks entering the free surface of a fluid. Physics of Fluids 10(10): 2489-2499. https://doi.org/10.1063/1.869787

Guo HP, Zou ZJ (2017) System-based investigation on 4-DOF ship maneuvering with hydrodynamic derivatives determined by RANS simulation of captive model tests. Applied Ocean Research 68: 11-25. https://doi.org/10.1016/j.apor.2017.08.006

ITTC Resistance Committee (2017) Uncertainty analysis in CFD Verification and validation methodology and procedures. ITTC-Recommended Procedures and Guidelines, 1-13

Karman V (1929) The impact of seaplane floats during landing. National Advisory Committee for Aeronautics, Washington DC, United States, NACA Technical Report No. NACA-TN-321

May A (1952) Vertical entry of missiles into water. Journal of Applied Physics 23(12): 1362-1372. https://doi.org/10.1063/1.1702076

Myring DF (1976) A theoretical study of body drag in subcritical axisymmetric flow. Aeronautical Quartely 27(3): 186-194. https://doi.org/10.1017/s000192590000768x

Pan C, Guo Y (2013) Design and simulation of ex-range gliding wing of high altitude air-launched autonomous underwater vehicles based on SIMULINK. Chinese Journal of Aeronautics 26(2): 319-325. https://doi.org/10.1016/j.cja.2013.02.008

Prasad BS, Sastry GRK, Das HN (2024) A comprehensive review study on multiphase analysis of water entry bodies. Ocean Engineering 292: 116579. https://doi.org/10.1016/j.oceaneng.2023.116579

Qi D, Feng J, Xu B, Zhang J, Li Y (2016) Investigation of water entry impact forces on airborne-launched AUVs. Engineering Applications of Computational Fluid Mechanics 10(1): 473-484. https://doi.org/10.1080/19942060.2016.1202864

Sahoo A, Dwivedy SK, Robi PS (2019) Advancements in the field of autonomous underwater vehicle. Ocean Engineering 181: 145-160. https://doi.org/10.1016/j.oceaneng.2019.04.011

Sener MZ, Aksu E (2022) The effects of head form on resistance performance and flow characteristics for a streamlined AUV hull design. Ocean Engineering 257: 111630. https://doi.org/10.1016/j.oceaneng.2022.111630

Shi HH, Itoh M, Takami T (2000) Optical observation of the supercavitation induced by high-speed water entry. J. Fluids Eng. 122(4): 806-810. https://doi.org/10.1115/1.1310575

Shi Y, Pan G, Yan GX, Yim SC, Jiang J (2019a) Numerical study on the cavity characteristics and impact loads of AUV water entry. Applied Ocean Research 89: 44-58. https://doi.org/10.1016/j.apor.2019.05.012

Shi Y, Pan G, Yim SC, Yan G, Zhang D (2019b) Numerical investigation of hydroelastic water-entry impact dynamics of AUVs. Journal of Fluids and Structures 91: 102760. https://doi.org/10.1016/j.jfluidstructs.2019.102760

Tan TJ, Hu J, Ge Y, Chen G, Yan Q (2019) Numerical simulation study on flow field distribution and load characteristics of trans-media aerial underwater vehicle during its water-exit process. Journal of Physics: Conference Series 1300(1): 012051. https://doi.org/10.1088/1742-6596/1300/1/012051

Truscott TT, Epps BP, Belden J (2014) Water entry of projectiles. Annual Review of Fluid Mechanics 46: 355-378. https://doi.org/10.1146/annurev-fluid-011212-140753

Wang X, Shi Y, Pan G, Chen X, Zhao H (2021) Numerical research on the high-speed water entry trajectories of AUVs with asymmetric nose shapes. Ocean Engineering 234: 109274. https://doi.org/10.1016/j.oceaneng.2021.109274

Wang YF, Wang Z, Du Y, Wang J, Wang Y, Huang C (2022) On the airflow in a cavity during water entry. International Journal of Multiphase Flow 151: 104073. https://doi.org/10.1016/j.ijmultiphaseflow.2022.104073

Wang YH (2012) Numerical modeling approach of an air-launched AUV initially impacting on water. Proceedings of the 2012 National Conference on Information Technology and Computer Science, Lanzhou, China, 336-340. https://doi.org/10.2991/citcs.2012.129

Wu J, Yang X, Xu S, Han X (2022) Numerical investigation on underwater towed system dynamics using a novel hydrodynamic model. Ocean Engineering 247: 110632. https://doi.org/10.1016/j.oceaneng.2022.110632

Yan GX, Pan G, Shi Y, Chao LM, Zhang D (2018) Experimental and numerical investigation of water impact on air-launched AUVs. Ocean Engineering 167: 156-168. https://doi.org/10.1016/j.oceaneng.2018.08.044

Yuan X, Xing T (2016) Hydrodynamic characteristics of a supercavitating vehicle's aft body. Ocean Engineering 114: 37-46. https://doi.org/10.1016/j.oceaneng.2016.01.012

Zhang T, Zhang R, Xing W, Lv X (2017) The numerical modeling approach of an air-launched AUV impacting into water. OCEANS 2017-Aberdeen, 1-5. https://doi.org/10.1109/OCEANSE.2017.8084703

Zhang W, Jia G, Wu P, Yang S, Huang B, Wu D (2021) Study on hydrodynamic characteristics of AUV launch process from a launch tube. Ocean Engineering 232: 109171. https://doi.org/10.1016/j.oceaneng.2021.109171

Zhang XY, Lyu XJ, Fan XD (2022) Numerical study on the vertical water exit of a cylinder with cavity. China Ocean Engineering 36(5): 734-742. https://doi.org/10.1007/s13344-022-0065-0

Zheng YN, Wang ZY, Wang GY (2020) Ventilated cavitating flow over a bluff body with special emphasis on the vortex-cavitation interaction. Ocean Engineering 217: 107925. https://doi.org/10.1016/j.oceaneng.2020.107925